PHYSICAL REVIEW B VOLUME 42, NUMBER 17 15 DECEMBER 1990-I

Tunneling-induced optical nonlinearities in asymmetric $Al_{0.3}Ga_{0.7}As/GaAs$ double-quantum-well structures

D. J. Leopold and M. M. Leopold
McDonnell Douglas Research Laboratories, P.O. Box 516, St. Louis, Missouri 63166
(Received 12 July 1990)

A photoluminescence study of the optical response in asymmetric, double-quantum-well structures is presented. The results reveal the existence of strong nonlinearities that can be attributed to electron and hole tunneling through the barrier layer. These nonlinearities arise from the difference between the electron and heavy-hole effective masses. The band bending resulting from spatial charge separation has a strong influence on the measured photoluminescence intensities for peaks associated with transitions between the lowest-energy electron and hole subband states in each quantum well. The system is strongly perturbed by an anticrossing of the second- and third-order heavy-hole subbands. Establishment of the heavy-hole resonant tunneling condition is shown to influence the intensities of the quantum-well photoluminescence peaks strongly. An effective-mass model of the double-quantum-well system reveals how the strength of these effects depends on both interwell coupling and the degree of structural asymmetry. This model successfully predicts the heavy-hole anticrossing observed in photoluminescence.

I. INTRODUCTION

Double-quantum-well (DQW) structures display many interesting properties not exhibited by single-quantum-well (SQW) structures. These properties are due to the finite potential barrier that separates the two constituent SQW's. The electron and hole tunneling through the finite barrier between the two SQW's makes DQW's attractive for fundamental studies of tunneling rates and mechanisms.[1–12] Since the DQW subband energy minima may be shifted, either by varying layer thicknesses and compositions or by applying a perpendicular electric field, both resonant and nonresonant tunneling processes may be examined. Further, the DQW system offers an opportunity to study many novel or enhanced electro-optic effects such as a stronger quantum-confined Stark effect compared with that of the SQW,[6,13–25] large oscillator strengths for "forbidden transitions" induced by perpendicular electric fields in symmetric and asymmetric structures,[19,26–28] and a blue shift of the absorption edge, again under application of a perpendicular electric field.[28–32] In many studies the barrier and well widths have been varied to determine how the electric field dependences of the electro-optical effects change with the strength of the interwell coupling. Some work has also been reported on nonlinear optical effects in electrically biased (*p-i-n* doped) DQW structures[33–38] and in electrically unbiased (undoped) DQW structures.[38–42] In the undoped structures strong nonlinearities arise from the difference between electron and heavy-hole tunneling rates or, equivalently, from the unequal confinements of the electrons and heavy holes in the coupled constituent SQW's.[39] Thus the nonlinearities are ultimately driven by the differences between the effective masses of carriers in the conduction and valence bands. Studies of nonlinear effects can be used to understand the competition between tunneling and recombination rates in DQW's. These studies may also lead to novel nonlinear photonic structures that exhibit bistability or even higher-order multistable states.

This paper will examine tunneling-induced nonlinear optical effects in electrically unbiased, asymmetric DQW structures in the $Al_{0.3}Ga_{0.7}As/GaAs$ system. These DQW structures exhibit two primary peaks in their photoluminescence (PL) spectra. Under weak excitation, the ratio of the low-energy PL peak intensity to the high-energy PL peak intensity is large. The nonlinearity shows up as a decrease in this ratio as the optical excitation level increases. This nonlinear effect is caused by electron and hole charge separation in the asymmetric DQW, which results in band bending and brings the two lowest conduction subband minima into resonance.[39] Calculations predict that the strength of the nonlinearity is sensitive to the magnitude of the structural asymmetry in the DQW. In addition, this asymmetry can be used to increase the heavy-hole tunneling rate by bringing two heavy-hole subbands into resonance. New data confirming this effect will be presented.

First, an effective-mass model of the asymmetric DQW will be presented. Calculations of subband quantum confinement energies and associated envelope wave functions for electrons and heavy holes reveal how the strength of the optical nonlinearity depends on both the interwell coupling and on the degree of structural asymmetry in the DQW. With regard to DQW asymmetries, the model also examines the role played by the anticrossing of the heavy-hole $n=2$ and $n=3$ subband energy minima and its implications for optical nonlinearities.

After a discussion of the DQW model, PL results measured as a function of optical excitation intensity will be presented for several DQW structures having different barrier widths. Thus the nonlinearity is studied as a function of interwell coupling and photoexcited charge density. These results on $Al_{0.3}Ga_{0.7}As/GaAs$ DQW's

 ©1990 The American Physical Society

support earlier work reported on the $In_{0.53}Ga_{0.47}As/InP$ system.[39] In addition, the present study is extended to show the effect of varying the structural asymmetry of the DQW. For this purpose the width (L_{z1}) of the narrowest quantum well is systematically varied. A new phenomenon is revealed in which the nonlinearity displays anomalous behavior for a critical value of L_{z1}. The effective-mass model of the DQW structure identifies resonant heavy-hole tunneling as the cause of this phenomenon and correctly predicts the critical L_{z1} value at which it occurs.

II. MODELING

In this section a model of the DQW system is presented and the mechanisms responsible for optical nonlinearities are discussed. The energies of the subband minima and their corresponding envelope functions for a DQW have been calculated by solving the Schrödinger equation for both electrons and holes within the effective-mass approximation,

$$\frac{-\hbar^2}{2m_b}\frac{d^2\psi_{bn}(z)}{dz^2}+V_b(z)\psi_{bn}(z)=E_{bn}\psi_{bn}(z) , \quad (1)$$

where z is the direction perpendicular to the quantum-well plane, $V_b(z)$ represents the bulk band-edge potential, and m_b is the effective mass. The subscript b specifies either e for electrons in the conduction band or hh for heavy holes in the valence band. Equation (1) admits multiple solutions for each band, which are labeled by the subband index n for both the energies E_{bn} and the envelope functions ψ_{bn}. The boundary conditions imposed at the interfaces demand continuity of both the envelope functions and the envelope-function derivatives divided by the masses. Also, a band-gap energy difference split of 62% and 38% between the conduction and valence bands is used at the $Al_{0.3}Ga_{0.7}As/GaAs$ interfaces. Exciton binding energies, although not discussed in this section, are used in the experimental section to compare PL peak positions with calculated transition energies.[43,44]

Figure 1 illustrates an asymmetric DQW potential used in the modeling calculations. The spatial profiles of the bulk band edges are labeled V_e for electrons in the conduction band and V_{hh} for heavy holes in the valence band. The widths of the two GaAs quantum wells in Fig. 1 are $L_{z1}=3.1$ nm and $L_{z2}=6.2$ nm, and the $Al_{0.3}Ga_{0.7}As$ barrier thickness is $L_B=5.0$ nm. The confinement energies and envelope functions of the first two subbands for both electrons and heavy holes are also shown in Fig. 1. The light-hole states are not shown since the optical nonlinearities discussed in this paper were only observed at low temperature, where the thermalized light-hole population in each quantum well is very small compared to the heavy-hole population. Since the two quantum wells in Fig. 1 are only weakly coupled, due to the moderately large barrier width, the energies of the subband minima differ only slightly from those of uncoupled SQW's. Thus the $n=1$ levels of the DQW (E_{e1} and E_{hh1}) are approximately equal to the $n=1$ levels of the wide SQW, and the $n=2$ levels of the DQW (E_{e2} and

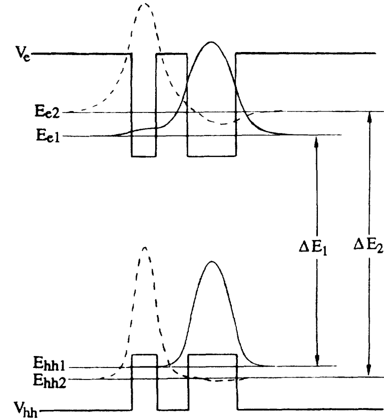

FIG. 1. Spatial profile of the conduction-band-edge energy V_e and valence-band-edge energy V_{hh} for an asymmetric, double-quantum-well structure. The confinement energies and wave functions of the ground state and first excited state for electrons (E_{e1} and E_{e2}) and heavy holes (E_{hh1} and E_{hh2}) in the quantum wells along with the primary optical transitions (ΔE_1 and ΔE_2) associated with these states are indicated.

E_{hh2}) are approximately equal to the $n=1$ levels of the narrow SQW.

The envelope functions displayed in Fig. 1 illustrate the relative degree of coupling between the wells. For instance, while both the $n=1$ electron and heavy-hole envelope functions (solid lines in Fig. 1) are localized primarily within the wide well, they also have significant amplitudes within the narrow well. In a similar manner, while the $n=2$ envelope functions (dashed lines in Fig. 1) are localized predominantly within the narrow well, they have finite amplitudes within the wide well. The electron envelope functions couple into the adjacent well more strongly than the heavy-hole envelope functions because of the smaller effective mass of the electron. This difference in coupling between the electrons and heavy holes causes the experimentally observed optical nonlinearities discussed in this paper and previously demonstrated in $In_{0.53}Ga_{0.47}As/InP$ DQW's.[39]

For the DQW system portrayed in Fig. 1, two primary optical transitions are observed in PL experiments. The lower-energy transition labeled ΔE_1 in Fig. 1 corresponds to recombination of the $n=1$ electron at energy E_{e1} with the $n=1$ heavy hole at energy E_{hh1}. The higher-energy transition, labeled ΔE_2 in Fig. 1, corresponds to recombination of the $n=2$ electron (E_{e2}) with the $n=2$ heavy hole (E_{hh2}). The envelope functions shown in Fig. 1 illustrate that the ΔE_1 and ΔE_2 transitions are characteristic of the wide and narrow wells, respectively, and that both transitions are spatially direct.

The response of the asymmetric DQW system to optical excitation differs markedly from that of a SQW system because of the coupling between the two wells. Because of this coupling, photoexcited electrons and holes in the narrow quantum well have two possible recombination channels rather than one. The carriers may recombine directly as in the SQW case by emitting a pho-

ton of energy ΔE_2 or they may tunnel into the wide well, lose energy through intraband relaxation, and then recombine by emitting a photon of lower energy ΔE_1. The competition between these two recombination channels is very sensitive to DQW design parameters. When the net tunneling rate from the narrow to the wide well is larger than the intrinsic SQW recombination rates, the PL peak intensity at energy ΔE_1 will be much larger than that at ΔE_2.

For the DQW design of Fig. 1, there is an important difference between the charge carrier dynamics of the conduction and valence bands. Because of the larger mass, heavy holes in the valence band cannot maintain the same tunneling current from the narrow to the wide well as electrons in the conduction band. As optical excitation intensity increases, causing larger steady-state electron and hole populations, a spatial separation of charge results with an excess of electrons in the wide well and an excess of holes in the narrow well. The dipole field created by the displaced electron and hole charges induces band bending. This band bending increases with excitation intensity and shifts the $n=2$ subband minima of the conduction band down in energy towards the $n=1$ level. At a high enough excitation, the $n=1$ and $n=2$ conduction subband minima become degenerate, a resonant tunneling condition is established, and the electron exchange rate between the two wells is enhanced. The band bending associated with increasing excitation intensity causes a nonlinearity in the PL spectra. Specifically, as the excitation increases, the PL intensity at energy ΔE_2 grows faster than that at energy ΔE_1.[39] As a result, the relative strengths of the PL peaks are excitation dependent. For this nonlinear effect to be observed the DQW must be designed so that a large electron and hole charge displacement can be established between the two wells. The resulting dipole field must be strong enough to produce sufficient band bending with moderate excitation intensities. Both the barrier width and the well widths must be properly chosen to achieve this.

An optimum barrier width is most easily chosen by examining modeling results of the DQW system. Figure 2 shows the dependence of the subband confinement energies on the barrier width L_B in the DQW system. Confinement energies for three conduction subbands are shown in Fig. 2(a) and confinement energies for five heavy-hole subbands are shown in Fig. 2(b). In both cases the zero of energy is taken as the bulk band edge and positive values of confinement energy represent how deep into the band the energies are shifted due to quantum confinement. The insets in Fig. 2 show the DQW potential profile for each band and also identify the relevant layer widths. The narrow well has width $L_{z1}=3.1$ nm and the wide well has width $L_{z2}=6.2$ nm, while the barrier thickness L_B is varied between zero and 10 nm. These DQW parameters correspond to the structures examined experimentally in Sec. III A.

Figure 2 can be used to design DQW's with strong optical nonlinearities by selecting values of L_B where coupling is present for electrons but not for heavy holes. This selection is accomplished by studying the subband energies and associated envelope functions between the two limiting cases of an "infinitely wide" barrier ($L_B > 10$ nm) and no barrier ($L_B=0$ nm). For "infinitely wide" barriers, where the two quantum wells are completely isolated, the DQW confinement energies are equal to the SQW confinement energies of the two constituent wells. Thus, for both the conduction and heavy-hole bands, the $n=1$ and $n=3$ DQW levels are equivalent to the $n=1$ and $n=2$ SQW levels for the wide well and the $n=2$ DQW level is equivalent to the $n=1$ SQW level for the narrow well. In the limit of zero barrier width the SQW case is also recovered, but with a composite well width of $L_z=L_{z1}+L_{z2}$. As the barrier width decreases below 10 nm the two independent wells begin to couple and carriers previously confined to one well can tunnel into the adjacent well. The presence of strong interwell coupling

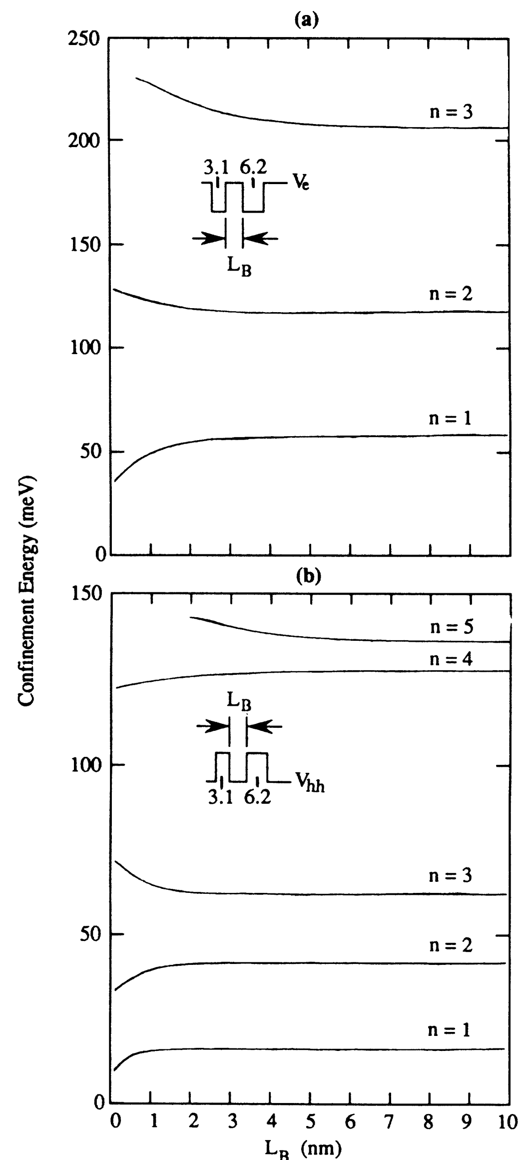

FIG. 2. Subband confinement energies for electrons (a) and heavy holes (b) in an asymmetric, $Al_{0.3}Ga_{0.7}As/GaAs$ double-quantum-well structure as shown in the inset. The index n labels the subband order. L_B is the barrier width.

is exemplified by measurable shifts in the subband confinement energies. In Fig. 2 the confinement energies exhibit very little sensitivity to changes in barrier width until L_B is decreased below a critical value. In the conduction band, barrier widths less than 3 nm are required before strong interwell coupling begins to significantly alter the confinement energies. The results presented in Fig. 2(a) are in agreement with earlier work reported on conduction-band confinement energies in asymmetric DQW's.[18] For the heavy-hole band, barrier widths less than 1 nm are required to significantly alter the confinement energies. Thus Fig. 2 shows that there exists an intermediate range of barrier widths where the electrons are strongly coupled but the heavy holes are not. This is one of the requirements for the observation of strong optical nonlinearities in the DQW system.

A second consideration for producing strong optical nonlinearities is to use as wide a barrier as possible while maximizing the differential electron and hole tunneling currents. Wide barriers produce larger potential drops between the quantum wells for the same separated charge density. Another point to consider in the DQW system is that interwell charge transfer occurs by nonresonant tunneling unless the subband levels are degenerate. To conserve momentum this process requires phonon participation if the concentration of impurities is low. Thus nonresonant electron tunneling can be enhanced by designing DQW's where the $n=1$ and $n=2$ subband energy separation is greater than the LO phonon energy. Since the LO phonon energy in GaAs is 36 meV, differential electron and hole spatial charge transfer from the narrow well to the wide well can be maximized in DQW structures if the electron subbands are separated by at least this energy.[2,3,5,8,10,12] Asymmetric DQW structures incorporating all of these design features should exhibit strong tunneling-induced optical nonlinearities.

While Fig. 2 displays the effect of barrier width on coupling, the DQW confinement energies also have a strong dependence on well width. In particular, a new phenomenon with significant implications for enhanced optical nonlinearities is revealed when L_{z1} is varied and L_{z2} is kept constant. The resulting structural asymmetry can cause the $n=2$ and $n=3$ heavy-hole confinement energies to converge and exhibit an anticrossing. Under this resonant condition the heavy-hole tunneling rate between the narrow well and the wide well increases dramatically, becoming comparable to the nonresonant electron tunneling rate. To exploit the heavy-hole resonant tunneling condition, it is important to know at what value of L_{z1} the anticrossing occurs.

In Fig. 3 are shown the calculated confinement energies for the case where the width of one quantum well, L_{z1}, of the DQW system is varied from zero to 10 nm while the width of the second quantum well is fixed at $L_{z2}=6.2$ nm and the barrier thickness is $L_B=5.1$ nm. These DQW parameters correspond to the structures measured experimentally in Sec. III B. Figure 3(a) shows the conduction subbands while Fig. 3(b) shows the heavy-hole subbands. The results presented in Fig. 3(a) for the conduction subbands are qualitatively similar to those reported earlier for $Al_{0.3}Ga_{0.7}As/GaAs$ DQW's.[18] As L_{z1} is made smaller or larger than L_{z2}, the asymmetry of the structure increases and the subband levels shift in energy. The functional dependence of each subband level on L_{z1} can be qualitatively understood in terms of the subband levels for the two individual constituent SQW's. Thus the plots of Fig. 3 can be considered to be composed of two plots, one for a SQW of width L_{z1} and another for a SQW of width L_{z2}. The subband levels of a SQW of width L_{z1} decrease in energy as L_{z1} increases, while the subband levels of a SQW of width L_{z2} are independent of L_{z1} and therefore appear as horizontal lines. The coupling between the wells (due to the finite barrier width) manifests itself as a series of anticrossings at each point where subband-level degeneracy occurs. The energy gaps that open at the conduction subband anticrossings are larger than those at the heavy-hole subband an-

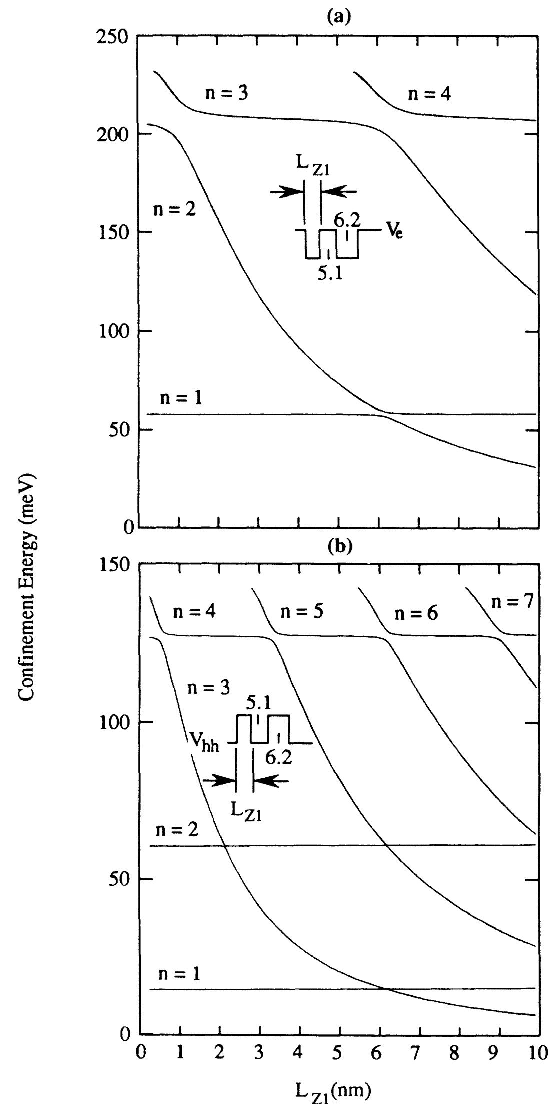

FIG. 3. Subband confinement energies for electrons (a) and heavy holes (b) in an asymmetric, $Al_{0.3}Ga_{0.7}As/GaAs$ double-quantum-well structure as shown in the inset. L_{z1} is the width of the first quantum well.

ticrossings because the conduction-band mass is smaller than the heavy-hole mass.

The dependence of the confinement energy on L_{z1} for a given subband changes abruptly as L_{z1} is increased from a value below an anticrossing to a value above it. For instance, if a given subband exhibits a strong functional dependence on L_{z1} for values below the anticrossing, it will abruptly change to being nearly constant for L_{z1} values greater than the anticrossing. This change is due to the envelope function for each subband switching from one well to another at these anticrossings. When the envelope function is localized mainly in the quantum well of width L_{z2} its confinement energy has only a weak dependence on L_{z1} and when the envelope function is localized mainly in the quantum well of width L_{z1} the dependence is strong.

The values of L_{z1} at which the anticrossings occur are specific to both the choice of band and the choice of subband except for the anticrossings which occur for all subbands at the $L_{z1}=L_{z2}$ symmetry point. In general, the different anticrossing points make possible the design of an asymmetric DQW structure in which two of the heavy-hole subbands are degenerate while the corresponding (same index n) conduction subbands are nondegenerate. An example of this can be seen in Fig. 3 for $L_{z1}=2.2$ nm, where the $n=2$ and $n=3$ heavy-hole subbands exhibit anticrossing behavior. At this point the $n=2$ and $n=3$ heavy-hole confinement energies of both levels are approximately equal, and resonant tunneling is established. Therefore the hole tunneling rate between the two quantum wells is expected to be relatively high compared to other cases where the heavy-hole states are essentially uncoupled. In contrast, the $n=2$ and $n=3$ conduction subbands display a much larger energy separation (several tens of meV) since the conduction-band anticrossing does not occur at $L_{z1}=2.2$ nm. Thus, for $L_{z1}=2.2$ nm, nonresonant tunneling occurs in the conduction band and resonant tunneling occurs in the valence band.

In the DQW system, an increase in tunneling rate at an anticrossing is accompanied by increased mixing of the envelope functions. Figure 4 shows quantitatively the change in envelope function shape that occurs as L_{z1} is varied. In this figure the solid lines represent the conduction-band envelope functions and the dashed lines represent the heavy-hole envelope functions. Envelope functions are plotted in each row for a different subband (labeled by the subband index n) and in each column for a different value of L_{z1}. In Fig. 4, column (a) has the widest L_{z1} (3.1 nm), column (b) has an intermediate L_{z1} (2.0 nm), and column (c) has the narrowest L_{z1} (1.0 nm). Figure 4 shows that the $n=1$ subband envelope functions for both the conduction and heavy-hole bands change very little with L_{z1} and are localized in the wide well for all values of L_{z1}. In contrast, the $n=2$ ($n=3$) envelope functions exhibit a dramatic change and shift from the narrow (wide) to the wide (narrow) well as L_{z1} decreases. Thus as an anticrossing region is approached the $n=2$ and $n=3$ envelope functions behave as a strongly coupled pair of states, primarily localized in opposite wells, that switch

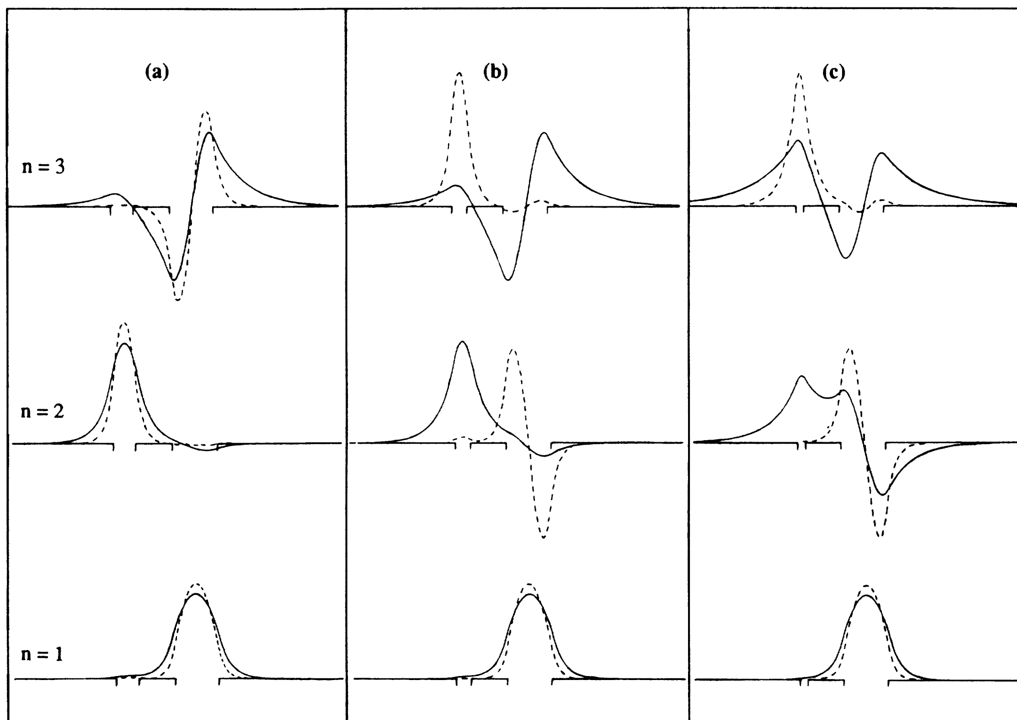

FIG. 4. Electron (solid lines) and heavy-hole (dashed lines) wave functions for the $n=1$, 2, and 3 subbands in an asymmetric, $Al_{0.3}Ga_{0.7}As/GaAs$ double-quantum-well structure having a barrier width of 5.1 nm and quantum-well widths (L_{z1}/L_{z2}) of (a) 3.1 nm/6.2 nm, (b) 2.0 nm/6.2 nm, and (c) 1.0 nm/6.2 nm.

wells as L_{z1} is decreased through a critical value. The envelope-function switch for heavy holes is a rapid function of L_{z1}. Figure 4 shows that complete switching occurs between $L_{z1}=3.1$ nm and $L_{z1}=2.0$ nm. This is consistent with the anticrossing point at $L_{z1}=2.2$ nm, which was previously identified through the use of Fig. 3. At this degenerate anticrossing the strongly coupled envelope functions for both the $n=2$ and $n=3$ subbands spread over both wells.

For electrons in the conduction band, the same qualitative trend is found. The $n=2$ electron envelope function shifts towards the wide well and the $n=3$ envelope function shifts towards the narrow well as L_{z1} decreases. However, the envelope-function switching occurs over a larger range of L_{z1} for electrons than it does for heavy holes, as Fig. 4 shows. Even for $L_{z1}=1.0$ nm the full transfer of the $n=2$ ($n=3$) electron envelope function to the wide (narrow) well is not complete. In fact, at $L_{z1}=1.0$ nm the $n=2$ and $n=3$ electron envelope functions have strong amplitudes in both wells, consistent with the location of the anticrossing in Fig. 3.

The strengths of optical transitions between the various subband states in the asymmetric DQW system are determined by the degree of spatial overlap between the initial- and final-state wave functions. Using effective-mass theory, the total wave function is separated into Bloch functions and envelope functions. The optical nonlinearities that can arise from asymmetries in the DQW system are most clearly shown by examining the envelope-function contribution to absorption and emission. Quantitatively, the intensity of an optical transition observed in PL is proportional to the square of the envelope-function overlap integral,

$$I \propto \left| \int_{-\infty}^{\infty} \psi^*_{\mathrm{hh}n}(z) \psi_{em}(z) dz \right|^2 , \quad (2)$$

where $\psi_{\mathrm{hh}n}(z)$ and $\psi_{em}(z)$ are the envelope functions of the nth heavy-hole subband and the mth conduction subband, respectively.

Figure 5 shows the square of the overlap integral for various pairs of subbands (up to third order) as L_{z1} is varied. Of the nine cases studied for these particular structural parameters, five have little impact on optical nonlinearities in the asymmetric DQW system. For example, the e3-hh1 and the e1-hh3 overlap integrals are essentially zero for all L_{z1} values. Thus these transitions have very little strength in optical experiments. Although the e1-hh1 transition along with the e2-hh1 and e1-hh2 transitions show some structure, it occurs only in the vicinity of the $L_{z1}=L_{z2}=6.2$ nm symmetry point where both the conduction-band and heavy-hole band envelope functions switch simultaneously between wells. The simultaneous switching of the overlap integrals for all subbands is not particularly interesting. The small variations in overlap integral near $L_{z1}=6.2$ nm are caused solely by differences in band offsets and effective masses for electrons and heavy holes.

The remaining four plots in the lower right corner of Fig. 5 show dramatic structure near $L_{z1}=2.2$ nm. The overlap integrals of the diagonal e2-hh2 and e3-hh3 transitions are large for $L_{z1}>2.2$ nm but decrease sharply for $L_{z1}<2.2$ nm. The opposite behavior is displayed by the off-diagonal transitions, e2-hh3 and e3-hh2, where the overlap integrals are zero for $L_{z1}>2.2$ nm and large for $L_{z1}<2.2$ nm. This very sharp transition of the overlap integrals near $L_{z1}=2.2$ nm is caused by envelope-function switching of the heavy-hole $n=2$ and $n=3$ subbands as previously discussed with reference to Fig. 4. As L_{z1} decreases from 2.4 to 1.9 nm, the envelope function for the $n=2$ heavy-hole level completely switches from the narrow well to the wide well and the $n=3$ subband envelope function does just the opposite. However, the conduction-band envelope functions are experiencing only minor spatial variations for L_{z1} values near 2.2 nm, i.e., the $n=2$ subband envelope function remains primarily in the narrow well and the $n=3$ subband envelope function remains mainly in the wide well. A switch of the $n=2$ heavy-hole envelope function from the narrow to the wide well (as L_{z1} decreases) results in large overlap integral changes with the $n=2$ conduction-band envelope function, as shown for the e2-hh2 transition near $L_{z1}=2.2$ nm in Fig. 5. Also, the shift of the $n=2$ heavy-hole subband envelope function to the wide well produces strong overlap with the $n=3$ conduction subband envelope function, as the box labeled e3-hh2 in Fig. 5 shows. Qualitatively similar results are found for transitions involving the $n=3$ heavy-hole subband. Calculated oscillator strengths between electron and hole subband states were previously reported in electrically unbiased, asymmetric $Al_{0.27}Ga_{0.73}As$/GaAs DQW structures.[27] However, the strong functional dependence shown in Fig. 5 was not found in these DQW structures. This difference can be attributed to the use of a much thinner barrier layer ($L_B=1.8$ nm) in the calculated oscillator strengths,[27] which allows the hole states to couple more strongly than in the present work. It is important to design DQW structures with strong electron coupling and weak hole coupling to maximize the effects of asymmetry.

The occurrence of these very sharp and relatively large changes in overlap integral in the vicinity of the $n=2$ to $n=3$ heavy-hole anticrossing is expected to affect PL experiments in three ways. First, the characteristic energy of the ΔE_2 transition illustrated in Fig. 1 is expected to change. The PL peak energy associated with the ΔE_2 transition will be determined by the $n=2$ electron confinement energy in conjunction with either the $n=2$ or $n=3$ heavy-hole confinement energy, depending on whether L_{z1} is greater or less than 2.2 nm. Second, and more important for optical nonlinearities, is the expectation that the intensity of the ΔE_2 transition observed in PL increase at $L_{z1}=2.2$ nm. This increase in intensity is a direct result of the stronger interwell coupling for heavy holes at the $L_{z1}=2.2$ nm anticrossing. Finally, increased tunneling of the heavy holes because of the resonant condition should inhibit the buildup of a spatial charge separation between the two quantum wells as optical excitation is increased. Without charge separation, excitation-dependent band bending does not occur, and since electron and hole tunneling currents then become comparable the nonlinear excitation intensity dependence

of the quantum-well peaks should be weak. However, the electron and hole tunneling rates will not be identical and some charge separation and nonlinear excitation dependence will occur. In fact, the band bending that results from stronger electron tunneling should drive the heavy-hole subbands in and out of resonance, producing additional nonlinear structure in the optical response of the system.

The modeling results presented in this paper have shown in part how optical nonlinearities in DQW's depend on both the interwell coupling, which is controlled by the choice of barrier width, and on the spatial asymmetry of the structure, which can be controlled by the choice of well widths. These modeling results were used to design a series of asymmetric DQW structures, which were then probed by use of PL spectroscopy.

III. EXPERIMENTAL RESULTS

A. Effect of interwell coupling

A series of asymmetric, coupled $GaAs/Al_{0.3}Ga_{0.7}As$ DQW structures were designed by making use of the calculated subband energies, envelope functions, and associ-

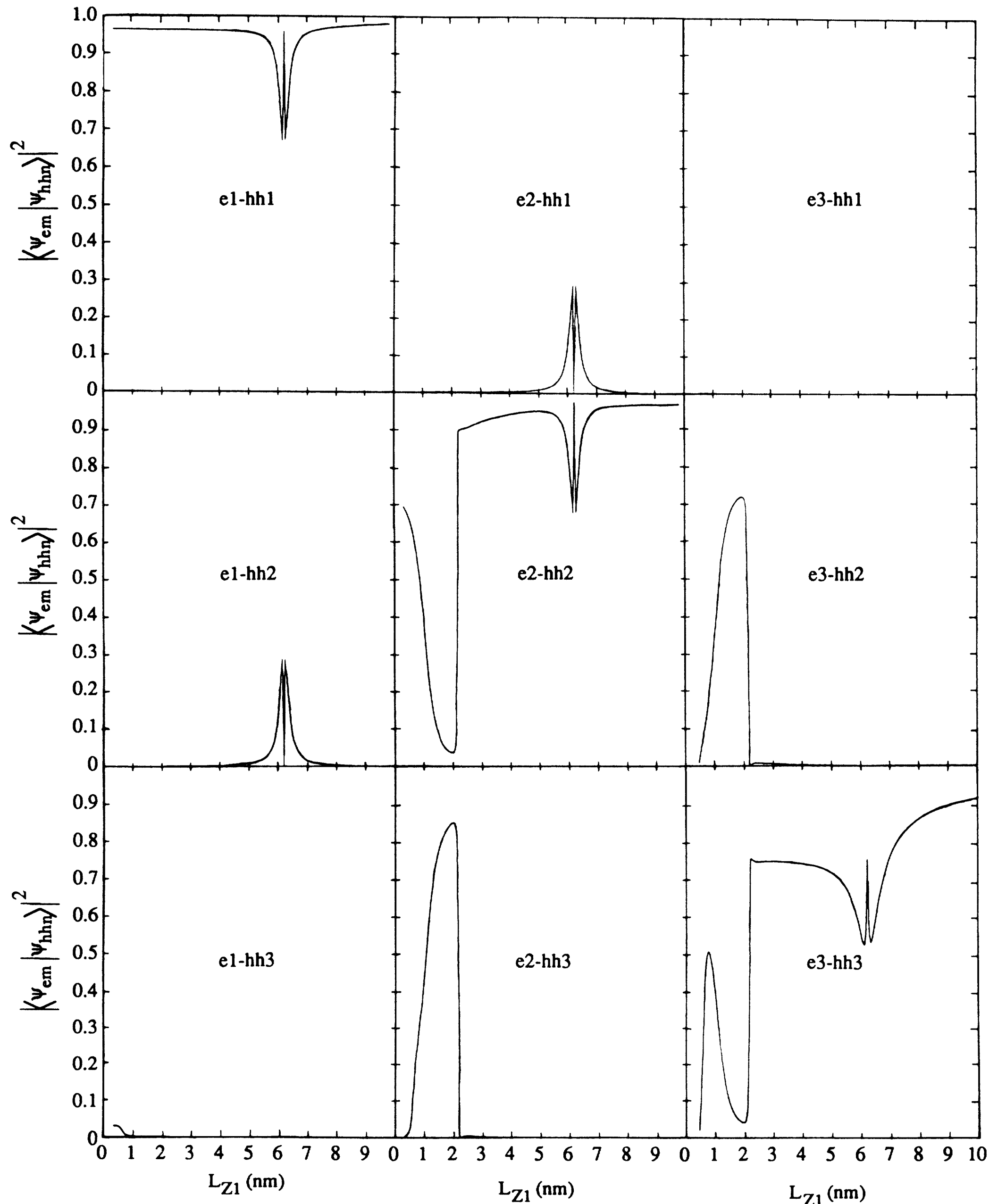

FIG. 5. Square of the electron-hole wave-function overlap integral between the $n=1$, 2, and 3 subband states for an asymmetric, $Al_{0.3}Ga_{0.7}As/GaAs$ double-quantum-well structure. The barrier thickness is 5.1 nm and one quantum well has a width of $L_{z2}=6.2$ nm while the width of the other quantum well, L_{z1}, is varied.

ated coupling strengths for electrons and heavy holes presented in Sec. II. In particular, DQW structures were designed to have barrier widths which allow sufficient electron coupling but very little heavy-hole coupling between the wells. The quantum-well widths were tailored to ensure that the energy separation between the $n=1$ and $n=2$ electron subband states is larger than the GaAs longitudinal-optical phonon energy (36 meV), thus permitting more effective phonon-assisted nonresonant electron tunneling from the narrow well to the wide well. The electron and hole confinement energies in all of the DQW structures designed for these experiments are plotted in Figs. 2 and 3. The DQW structures were grown by molecular-beam epitaxy (MBE) on undoped (100)-oriented GaAs substrates.

All of the DQW structures were probed optically at 8, 77, and 300 K by use of PL spectroscopy. An argon-ion laser operating at 488 nm was used to photoexcite electron-hole pairs in the $Al_{0.3}Ga_{0.7}As$ cladding layers in these structures. Most of these photoexcited carriers are captured in the GaAs quantum-well region before recombining through the transitions labeled ΔE_1 and ΔE_2 in Fig. 1. The PL emission was spectrally resolved and detected by use of a double-grating monochromator in combination with a cooled GaAs photomultiplier. The primary optical transitions illustrated in Fig. 1 for asymmetric DQW's show up clearly as two peaks in each of the four PL spectra displayed in Fig. 6. These four spectra were measured at 8 K using different laser excitation intensities. This asymmetric structure consists of two GaAs quantum wells of unequal thickness (3.1 and 6.2 nm) separated by a thin $Al_{0.3}Ga_{0.7}As$ (7-nm) barrier. In addition to GaAs and $Al_{0.3}Ga_{0.7}As$ bound exciton and carbon acceptor peaks, two strong quantum-well peaks are observed in each spectrum shown in Fig. 6. The shorter wavelength PL peak labeled $n=2$ near 740 nm and the longer wavelength peak labeled $n=1$ near 780 nm are attributed to transitions between states associated with the narrow and wide quantum wells, respectively. The $n=1$ PL peak arises from the spatially direct ground-state transition and the $n=2$ PL peak arises from the first excited-state transition. As optical excitation intensity is increased [Figs. 6(a)–6(d)] the relative strength of the $n=2$ transition approaches that of the $n=1$ transition. To further quantify this, the $n=1$ and $n=2$ quantum-well PL peak intensities measured as a function of excitation intensity are plotted in Fig. 7 for two, asym-

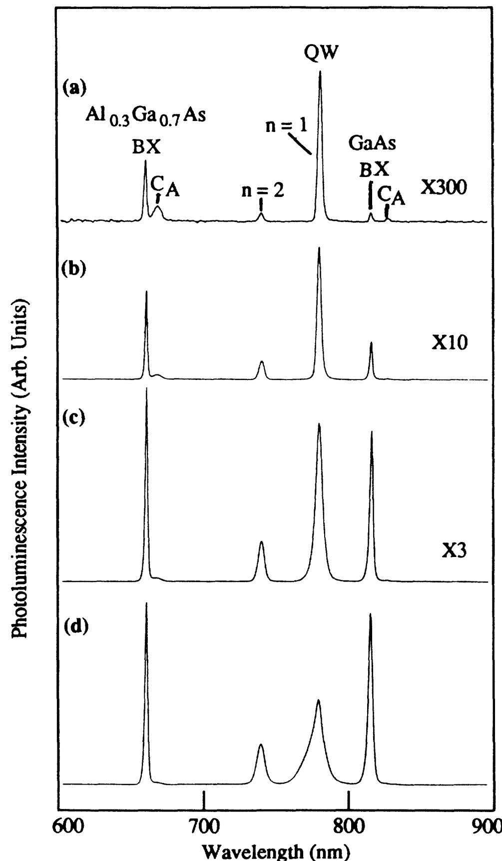

FIG. 6. Photoluminescence spectra measured at 8 K in an asymmetric $Al_{0.3}Ga_{0.7}As/GaAs$ double-quantum-well structure similar to that illustrated in Fig. 1. Two quantum-well peaks arising from the ground-state ($n=1$) and first excited-state ($n=2$) transition are shown, along with peaks associated with the $Al_{0.3}Ga_{0.7}As$ and GaAs layers. The laser excitation intensities used were (a) 6.4×10^{-4} W/mm^2, (b) 1.0×10^{-2} W/mm^2, (c) 6.4×10^{-2} W/mm^2, and (d) 2.0×10^{-1} W/mm^2.

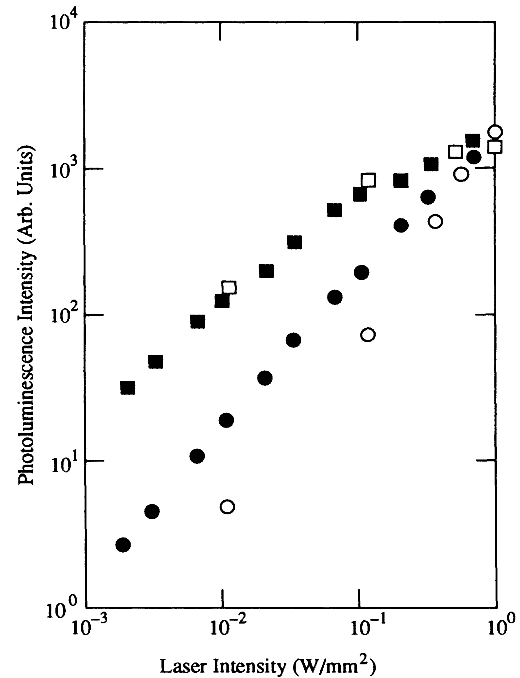

FIG. 7. Photoluminescence peak intensities measured at 8 K in two asymmetric $Al_{0.3}Ga_{0.7}As/GaAs$ double-quantum-well structures having well widths of 3.1 and 6.2 nm. The barrier widths are 6 nm (open symbols) and 7 nm (solid symbols). The square symbols are measured photoluminescence intensities for the ground state ($n=1$) transition while the circles are measured intensities for the excited-state ($n=2$) transition.

metric DQW samples having well widths of 3.1 and 6.2 nm. The barrier widths for the structures are 6 nm (open symbols in Fig. 7) and 7 nm (solid symbols in Fig. 7). The squares in Fig. 7 represent PL intensity (I_1) arising from the ground-state (e1-hh1) transition in each structure while the circles represent PL intensity (I_2) from the first excited-state (e2-hh2) transition. As expected, PL arising from the ground-state transition is stronger than that from the first excited state, and the intensity differences (I_1-I_2) are larger for the structure having the thinner $Al_{0.3}Ga_{0.7}As$ barrier separating the two GaAs quantum wells. The total integrated PL intensity arising from the quantum-well region (I_1+I_2) is nearly the same for the two structures and exhibits a linear dependence on laser power for low excitation intensities. As concluded in earlier work[39] on $In_{0.53}Ga_{0.47}As/InP$, the PL intensity differences observed in the spectra of Fig. 6 and plotted in Fig. 7 are attributed to electron and hole tunneling between the two coupled quantum wells since structures having very wide (>15 nm) barriers show no appreciable changes in relative intensity. The PL peak intensity ratios (I_1/I_2) for the quantum-well transitions in DQW structures having fixed well widths ($L_{z1}=3.1$ nm and $L_{z2}=6.2$ nm) and three different barrier dimensions (5, 6, and 7 nm) are plotted in Fig. 8. As optical excitation power increases, the PL intensity ratio approaches unity for all samples. For a constant optical excitation power density, wider barriers give rise to smaller intensity ratios. The PL intensity dependence observed in these

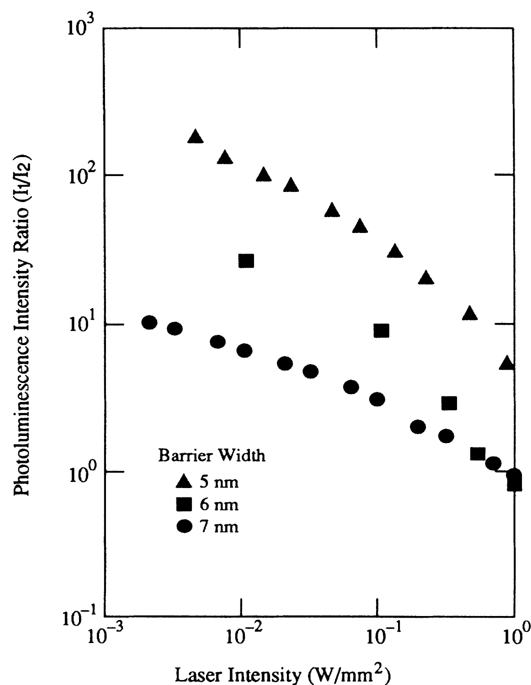

FIG. 8. Photoluminescence intensity ratios ($I_{n=1}/I_{n=2}$) measured as a function of incident laser power density in asymmetric, $Al_{0.3}Ga_{0.7}As/GaAs$ double-quantum-well structures having 3.1- and 6.2-nm-thick quantum wells separated by barrier layers having widths of 5, 6, and 7 nm as indicated.

$GaAs/Al_{0.3}Ga_{0.7}As$ DQW structures is similar to that reported in $In_{0.53}Ga_{0.47}As/InP$.[39] Also, the measured PL intensity ratio dependence on barrier width closely matches that measured in $Al_{0.26}Ga_{0.74}As/GaAs$ DQW's (Ref. 10) and in AlAs/GaAs DQW's.[40] In the latter system thinner barriers are required to observe significant tunneling effects since the barrier potential is higher in AlAs than it is in the alloy. Thin barriers make it harder to establish sufficient band bending in the DQW structure, thus reducing the nonlinear optical response of the AlAs/GaAs system. This is the likely reason a weak nonlinear PL intensity dependence on excitation power is found in AlAs/GaAs DQW's.[40]

The variation in PL intensity ratios between the three structures shown in Fig. 8 can be explained by the differences in tunneling rates between electrons and holes from the narrow well to the wide well. This tunneling-induced effective-mass filtering effect results in charge separation as discussed previously. The dipole field produces band bending in a direction which reduces the energy separation between the $n=1$ and $n=2$ electron subband states. As the electronic subband state degeneracy is approached at high excitation intensity, the electron tunneling currents between the wide and narrow quantum wells become equal and the PL arising from the two wells is nearly equivalent. Thus excitation-dependent saturation of the PL intensity ratio is a signature of subband alignment and the establishment of resonant tunneling.[39,41]

The $n=1$ and $n=2$ subband level population distribution is not thermalized at low excitation levels for PL data shown in Fig. 8. This conclusion is drawn from the fact that no significant differences in PL intensity ratio were found between 8 and 77 K in these structures.[41] The thermal activation energy involved in this process is half of the energy separation between the measured $n=1$ and $n=2$ subband PL peaks, which is 87 meV in these structures. Thus, for barrier widths between 5 and 7 nm, the temperature-independent PL intensity ratios found below 77 K indicate that carriers captured in the narrow quantum well either recombine directly with energy ΔE_2 or tunnel into the wide well and recombine at a lower energy (ΔE_1) without significant backtunneling.[41] Thermalized population distributions were important at 300 K, where the PL peak intensity ratios for all of the structures became much smaller.

Optical hysteresis has been predicted in asymmetric DQW structures.[39] The mechanism driving the bistability is expected to be a switching between resonant and nonresonant tunneling as the electron subband states becomes degenerate due to band bending. The DQW structures presented in this paper were examined for optical bistability. A small hysteresis effect was observed at 8 K for the $n=2$ electron–to–heavy-hole transition. A slightly larger effect was measured for the $n=2$ electron–to–light-hole transition, although the PL intensity was much smaller. This noticeable hysteresis difference is attributed to band bending, which can switch the light hole from a bound state to a quasibound state and allow the light hole to escape from the quantum-well region entirely.

B. Effect of structural asymmetry

The degree of asymmetry built into the DQW structure can result in subband-level anticrossings as discussed in the modeling section and illustrated in Figs. 3–5. The occurrence of subband-level degeneracy and associated envelope wave function switching can be expected to alter the optical properties of DQW structures both by changing the tunneling rates through the barrier layer and by altering the transition oscillator strengths between the different pairs of subbands involved at an anticrossing. Thus the strongest optical transition involved would be expected to switch from one pair of subbands to a different pair as an anticrossing point is approached.

Four DQW samples were fabricated to study the effects of subband anticrossing. Each DQW structure consisted of a 6.2-nm-wide GaAs quantum well and a 6-nm-thick $Al_{0.3}Ga_{0.7}As$ barrier layer. The width of the narrow quantum well (L_{z1}) was varied over a range which encompassed the $n=2$ and $n=3$ heavy-hole anticrossing illustrated in Fig. 3. As with previous DQW structures, the measured PL spectra for each sample exhibited two strong peaks associated with the quantum-well region. However, some significant changes occurred in the PL spectra for this series of structures where the narrow quantum-well width (L_{z1}) passed through the heavy-hole anticrossing region. Both the measured PL peak positions and the intensity ratios exhibited behavior characteristic of heavy-hole subband anticrossing.

Figure 9 presents the measured PL peak energies as a function of the narrow quantum-well width in the DQW structure. The solid lines in Fig. 9 represent the calculated transition energies between pairs of electron and heavy-hole subband states (en-hh$n$) having the same index n. The dashed line in Fig. 9 is the calculated transition energy between the $n=2$ electron and $n=3$ heavy-hole subbands ($e2$-hh3). In this series of samples, the lowest-energy quantum-well PL peak was found to be insensitive to changes in L_{z1}. As expected, this low-energy PL peak tracks the energy dependence of the ground-state transition ($e1$-hh1) associated with the wide quantum well. The PL response was quite different for the high-energy peak measured in the four DQW samples. This PL peak follows the $e2$-hh2 transition energy dependence on L_{z1} down to the heavy-hole anticrossing near $L_{z1}=2.2$ nm and then switches to the $e2$-hh3 dependence for $L_{z1}<2.2$ nm. This behavior is expected on theoretical grounds since the overlap integrals (Fig. 5) for the $e2$-hh2 and $e2$-hh3 transitions change abruptly near $L_{z1}=2.2$ nm. The slight deviation of some experimental points from the theoretical results in Fig. 9 can be explained by one monolayer thickness variations in calculating the quantum-well widths based on MBE growth rates and shutter times.

An additional signature of the heavy-hole anticrossing is found by examining the PL intensity ratios (I_1/I_2), which are plotted in Fig. 10. The PL intensity ratios for each of the four samples having different L_{z1} thicknesses exhibit a dependence on laser excitation intensity that is similar to that plotted in Fig. 8 for other asymmetric DQW structures. However, the PL intensity ratio (I_1/I_2) dependence on L_{z1} exhibits anomalous behavior at the $L_{z1}=2.2$ nm heavy-hole anticrossing. In general, reducing L_{z1} causes the PL intensity ratio to increase.

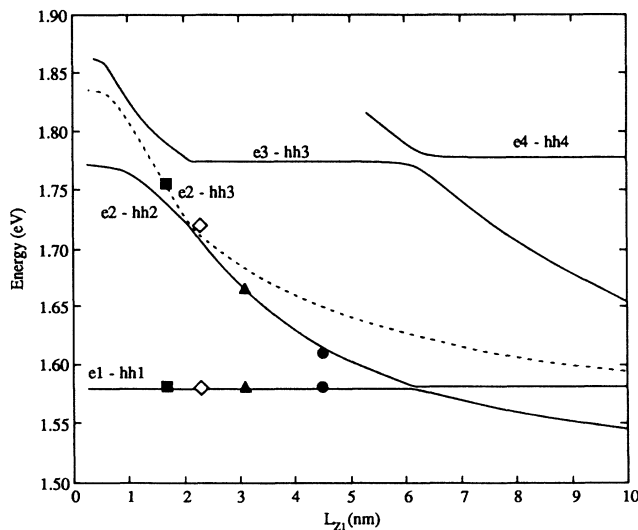

FIG. 9. Photoluminescence peak energies measured at 8 K in four asymmetric, $Al_{0.3}Ga_{0.7}As$/GaAs double-quantum-well structures as indicated. The solid lines are calculated transition energies between pairs of electron and heavy-hole subband states (en-hh$n$) having the same index n. The dashed line is the calculated transition energy between the $n=2$ electron and $n=3$ heavy-hole subbands ($e2$-hh3).

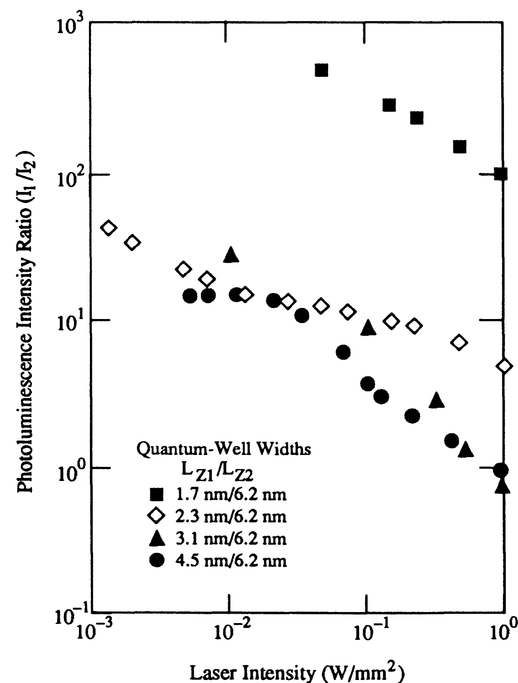

FIG. 10. Photoluminescence intensity ratios ($I_{n=1}/I_{n=2}$) measured as a function of incident laser power density in asymmetric, $Al_{0.3}Ga_{0.7}As$/GaAs double-quantum-well structures having quantum-well widths as indicated and a barrier layer thickness of 6 nm.

Thus the relative carrier population in the wide quantum well is enhanced as the narrow quantum-well width is reduced. This overall trend is a direct result of reduced carrier localization for subband states having a higher energy due to decreased well widths, which leads to higher tunneling currents from the narrow quantum well to the wide quantum well. The anomalous behavior found in the structure having a narrow quantum-well width of 2.3 nm is exemplified by significantly lower PL intensity ratios than expected for low excitation levels. This DQW structure represents the case where the $n=2$ and $n=3$ heavy-hole levels become degenerate and strongly couple. The strong resonant coupling of the two heavy-hole states in this sample causes the intensity of the narrow quantum-well PL peak to increase relative to the wide quantum-well PL peak. Both the hh2 and hh3 subbands actively participate in recombination with $e2$ at the anticrossing point. Thus establishment of heavy-hole resonant tunneling enhances the strength of the narrow quantum-well radiative recombination transitions ($e2$-hh2 and $e2$-hh3). Since nonresonant electron tunneling remains stronger than resonant heavy-hole tunneling, the band bending in the quantum-well region continues to follow the displaced electron and hole charge distributions as it did in previous samples. This band bending causes the DQW system to pass through the heavy-hole resonant tunneling condition as the optical excitation intensity is increased, and results in the PL intensity ratio plateau region observed in Fig. 10 for the structure with $L_{z1}=2.3$ nm. The PL intensity ratio "minimum" for this structure corresponds to the heavy-hole resonant tunneling case. The anomalous behavior of the PL intensity ratio for the structure with $L_{z1}=2.3$ nm cannot be explained by impurities or unintentional doping of the quantum wells since all of the DQW samples were prepared in a similar manner by MBE with the dopant effusion cells cold. These undoped samples have background impurity concentrations below 5×10^{14} cm^{-3}. The combined experimental data presented in Figs. 9 and 10 support the theoretical prediction that the heavy-hole levels cross at $L_{z1}=2.2$ nm in the series of DQW structures examined in this study.

IV. CONCLUSIONS

The $Al_{0.3}Ga_{0.7}As/GaAs$ DQW system exhibits optical nonlinearities that depend on both the strength of coupling between the quantum wells and the degree of asymmetry associated with the structure. The nonlinearities show up as large intensity changes observed in quantum-well PL peaks, and these changes are attributed to band bending caused by tunneling currents and a transition from nonresonant to resonant heavy-hole tunneling. Tunneling-induced effective-mass filtering causes a space charge buildup as optical excitation intensity is increased. The resultant dipole field bends the bands until the $n=1$ and $n=2$ electron subband states become degenerate and tunneling between the two quantum wells becomes symmetric. Under these conditions the PL intensity ratio for the peaks associated with the subbands approaches unity. The design of a DQW structure where two heavy-hole states become degenerate based on an effective-mass model is shown to significantly alter the PL intensity ratio. The heavy-hole resonant tunneling condition has a strong effect on the band bending as well as on optical recombination strengths for transitions involving these subband states.

ACKNOWLEDGMENTS

We wish to thank G. W. Bryant for many useful discussions and K. M. Borawski for help with the sample growths. This research was supported by the McDonnell Douglas Independent Research and Development program.

[1]D. F. Nelson, R. C. Miller, D. A. Kleinman, and A. C. Gossard, Phys. Rev. B **34**, 8671 (1986).
[2]T. Weil and B. Vinter, J. Appl. Phys. **60**, 3227 (1986).
[3]H. W. Liu, R. Ferreira, G. Bastard, C. Delalande, J. F. Palmier, and B. Etienne, Appl. Phys. Lett. **54**, 2082 (1989).
[4]Y. Zohta, T. Nozu, and M. Obara, Phys. Rev. B **39**, 1375 (1989).
[5]D. Y. Oberli, J. Shah, T. C. Damen, C. W. Tu,, T. Y. Chang, D. A. B. Miller, J. E. Henry, R. F. Kopf, N. Sauer, and A. E. DiGiovanni, Phys. Rev. B **40**, 3028 (1989).
[6]T. B. Norris, N. Vodjdani, B. Vinter, C. Weisbuch, and G. A. Mourou, Phys. Rev. B **40**, 1392 (1989).
[7]F. Sasaki and Y. Masumoto, Phys. Rev. B **40**, 3996 (1989).
[8]N. Sawaki, R. A. Höpfel, E. Gornik, and H. Kano, Appl. Phys. Lett. **55**, 1996 (1989).
[9]M. G. W. Alexander, M. Nido, K. Reimann, W. W. Rühle, and K. Köhler, Appl. Phys. Lett. **55**, 2517 (1989).
[10]F. Clerot, B. Deveaud, A. Chomette, A. Regreny, and B. Sermage, Phys. Rev. B **41**, 5756 (1990).
[11]M. Nido, M. G. W. Alexander, W. W. Rühle, T. Schweizer, and K. Köhler, Appl. Phys. Lett. **56**, 355 (1990).
[12]D. Y. Oberli, J. Shah, T. C. Damen, J. M. Kuo, J. E. Henry, J. Lary, and S. M. Goodnick, Appl. Phys. Lett. **56**, 1239 (1990).
[13]M. N. Islam, R. L. Hillman, D. A. B. Miller, D. S. Chemla, A. C. Gossard, and J. H. English, Appl. Phys. Lett. **50**, 1098 (1987).
[14]E. J. Austin and M. Jaros, J. Phys. C **19**, 533 (1986).
[15]Y. J. Chen, E. S. Koteles, B. S. Elman, and C. A. Armiento, Phys. Rev. B **36**, 4562 (1987).
[16]H. Q. Le, J. J. Zayhowski, and W. D. Goodhue, Appl. Phys. Lett. **50**, 1518 (1987).
[17]S. R. Andrews, C. M. Murray, R. A. Davies, and T. M. Kerr, Phys. Rev. B **37**, 8198 (1988).
[18]P. Yuh and K. L. Wang, Phys. Rev. B **38**, 8377 (1988).
[19]J. E. Golub, P. F. Liao, D. J. Eilenberger, J. P. Harbison, L. T. Florez, and Y. Prior, Appl. Phys. Lett. **53**, 2584 (1988).
[20]R. P. Leavitt, J. W. Little, and S. C. Horst, Phys. Rev. B **40**, 4183 (1989).
[21]C. C. Phillips, R. Eccleston, and S. R. Andrews, Phys. Rev. B **40**, 9760 (1989).
[22]D. Ahn, IEEE J. Quantum Electron. **25**, 2260 (1989).
[23]N. Debbar, S. Hong, J. Singh, P. Bhattacharya, and R. Sahai,

J. Appl. Phys. **65**, 383 (1989).
[24]R. P. Leavitt and J. W. Little, Phys. Rev. B **41**, 5174 (1990).
[25]W. L. Bloss, J. Appl. Phys. **67**, 1421 (1990).
[26]J. W. Little and R. P. Leavitt, Phys. Rev. B **39**, 1365 (1989).
[27]J. Lee, M. O. Vassell, E. S. Koteles, and B. Elman, Phys. Rev. B **39**, 10 133 (1989).
[28]Y. Tokuda, K. Kanamoto, Y. Abe, and N. Tsukada, Phys. Rev. B **41**, 10 280 (1990).
[29]K. K. Choi, B. F. Levine, C. G. Bethea, J. Walker, and R. J. Malik, Phys. Rev. B **39**, 8029 (1989).
[30]C. Cacciatore, D. Campi, C. Cariasso, C. Rigo, and C. Alibert, Phys. Rev. B **40**, 6446 (1989).
[31]H. Onose, H. Yoshimura, and H. Sakaki, Appl. Phys. Lett. **54**, 2221 (1989).
[32]D. Campi and C. Alibert, Appl. Phys. Lett. **55**, 454 (1989).
[33]J. W. Little, J. K. Whisnant, R. P. Leavitt, and R. A. Wilson, Appl. Phys. Lett. **51**, 1786 (1987).
[34]C. Weber, K. H. Schlaad, C. Klingshirn, C. v. Hoof, G. Borghs, G. Weimann, W. Schlapp, and H. Nickel, Appl. Phys. Lett. **54**, 2432 (1989).
[35]Y. Tokuda, K. Kanamoto, N. Tsukada, and T. Nakayama, J. Appl. Phys. **65**, 2168 (1989); Appl. Phys. Lett. **54**, 1232 (1989).
[36]Y. Tokuda, K. Kanamoto, and N. Tsukada, Appl. Phys. Lett. **56**, 166 (1990).
[37]D. A. B. Miller, Appl. Phys. Lett. **54**, 202 (1989).
[38]J. Khurgin, Appl. Phys. Lett. **51**, 2100 (1987); Phys. Rev. B **38**, 4056 (1988); Appl. Phys. Lett. **53**, 779 (1988); **54**, 2589 (1989).
[39]R. Sauer, K. Thonke, and W. T. Tsang, Phys. Rev. Lett. **61**, 609 (1988).
[40]T. Tada, A. Yamaguchi, T. Ninomiya, H. Uchiki, T. Kobayashi, and T. Yao, J. Appl. Phys. **63**, 5491 (1988).
[41]R. Sauer, T. D. Harris, and W. T. Tsang, Phys. Rev. B **39**, 12 929 (1989).
[42]M. G. W. Alexander, W. W. Rühle, R. Sauer, and W. T. Tsang, Appl. Phys. Lett. **55**, 885 (1989).
[43]E. S. Koteles and J. Y. Chi, Phys. Rev. B **37**, 6332 (1988).
[44]T. Kamizato and M. Matsuura, Phys. Rev. B **40**, 8378 (1989).